JOURNAL OF PROPULSION AND POWER
Vol. 27, No. 3, May–June 2011

# In Situ Thermal Characterization of the Accelerator Grid of an Ion Thruster

C. Bundesmann,* M. Tartz,† F. Scholze,† and H. Neumann†
*Leibniz-Institut für Oberflächenmodifizierung, e.V., 04318 Leipzig, Germany*
H. J. Leiter‡
*Astrium Space Transportation, GmbH, 74215 Moeckmuehl, Germany*
and
F. Scortecci§
*Aerospazio Tecnologie, s.r.l., 53040 Siena, Italy*

DOI: 10.2514/1.50049

**The application of an electric propulsion diagnostic system for in situ thermal characterization of electric thrusters is studied, as described previously. Exemplarily, the surface temperature profile of the accelerator grid of a gridded ion thruster RIT-22 is obtained and characterized. In situ pyrometer line scans in combination with precise measurements of geometrical grid parameters are demonstrated. The accelerator grid surface temperature of the firing thruster is obtained by a model calculation that requires the knowledge of geometrical grid parameters, such as hole diameter, distance between holes, or grid shape. These parameters are also measured in situ with a telemicroscope for high-resolution optical imaging and a triangular laser head for surface profile scanning. The distance between grid surface and pyrometer optics are precisely monitored with the support of the triangular laser head, for which the position is fixed with respect to the pyrometer. The distance measurement allows for correcting the measurement spot size of the pyrometer. The temperature profiles at three different beam power levels (1250, 2250, and 4000 W), and warm-up and cool-down phases demonstrate the capabilities of the complex equipment. It is found that thermal steady state is reached after 4 h of thruster firing. Furthermore, it is shown that the accelerator grid surface temperature increases almost linearly with increasing beam current.**

## Introduction

ELECTRIC propulsion (EP) is a key technology for space missions. Its advantage compared with other propulsion technologies (in particular, chemical propulsion) is the high exhaust velocity of the propellant. Thus, the amount of propellant needed for a space mission is smaller and, consequently, the launch mass is reduced [1–3]. So far, EP thrusters are mainly used for station-keeping, but their application for deep-space missions has also been demonstrated [4].

All thrusters undergo an extensive acceptance test program before flying in space. Even more tests are needed during the development phase when the thruster is optimized. EP thrusters are designed for a lifetime of up to several 10,000 h. During ground tests of engines, operation as long as their designed lifetime plus an additional margin of up to 50% is required. Several parameters are measured and should be optimized during the test phase: for instance, thermal properties. Thermal analysis provides essential performance data which also serve as input or validation data for thermal modeling of the thruster.

Recently, we described a diagnostic system for in situ characterization of EP thrusters [5] that can be employed for characterizing the surface temperature of EP thrusters. The characterization of the surface temperature of the accelerator grid of gridded ion thrusters is exemplarily demonstrated in our new investigation. This is done by combining pyrometer line scans and precise in situ measurements of geometrical grid parameters. Thermal characterization and modeling of gridded ion thrusters has been reported by several groups: first in the 1970s for mercury ion thrusters [6–8], and recently for Xe ion thrusters NASA Solar Electric Propulsion Technology Application Readiness (NSTAR) [9–12] and NASA Exploration Team (NEXT) [13,14]. The temperature of various thruster parts were measured by thermocouples and modeled. Even thermal environmental tests were performed. However, the reported experimental grid temperature data are restricted to parts far away from the grid hole area, i.e., the accelerator grid ring [9–11] or the accelerator and screen grid support [13,14]. No experimental data of the temperature distribution of the grids have been published yet. Only selected analytical temperature data for the accelerator and screen grid assembly were reported in [6,8]. The lack of experimental grid temperature data is due to the fact that thermocouple measurements in the center of the grid of a firing thruster are not possible, because these measurements require mechanical and electrical contacts. We describe how the accelerator grid temperature across the whole diameter of a firing thruster can be obtained from in situ optical pyrometer line scans. This technique does not require mechanical or electrical contacts. However, the grid temperature is difficult to measure because of the limited lateral resolution of the pyrometer optics at reasonable working distances. To extract the grid temperature from the measured pyrometer data, a model calculation is proposed. The model calculation requires the knowledge of geometrical grid parameters and the pyrometer spot size. The geometrical grid parameters are measured in situ with a telemicroscope for high-resolution optical imaging and a triangular laser head (TLH) for surface profile scanning. The pyrometer spot size can be determined from distance measurements by the TLH. The capabilities of our system are exemplarily demonstrated for a gridded ion thruster RIT-22.

## Experimental

The EP diagnostic system is shown in Fig. 1. It uses a high-precision five-axes positioning system mounted on a modular bar setup [5]. Three linear and two rotation tables allow us to position thruster and diagnostic tools very precisely, relative to each other.

Received 25 March 2010; revision received 27 January 2011; accepted for publication 27 January 2011. 

*Permoserstrasse 15; carsten.bundesmann@iom-leipzig.de (Corresponding Author).
†Permoserstrasse 15.
‡Post Box 1119.
§Zona Industriale Sentino, Rapolano Terme.

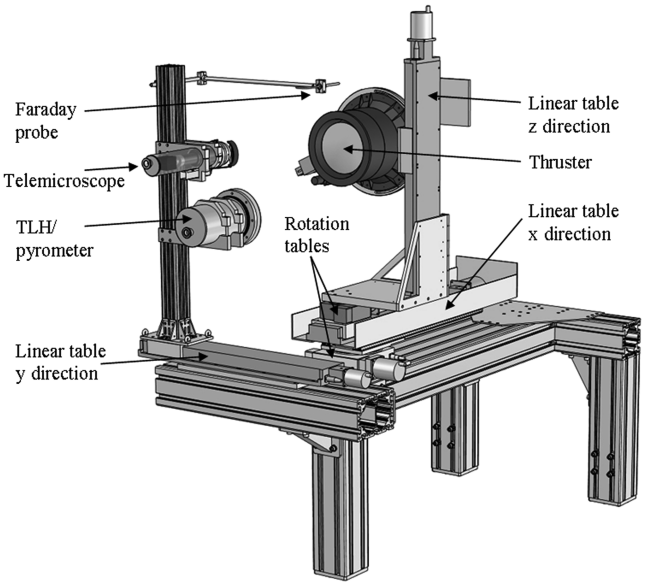


**Fig. 1 Diagnostic system setup [8]. Diagnostic tools are in parking position.**

The positioning reproducibility is better than 0.1 mm. Horizontal or vertical line scans, as well as two-dimensional and three-dimensional scans, are also possible. Three diagnostic tools are employed in this study: a pyrometer, a telemicroscope, and a TLH.

The temperature measurements are done with a pyrometer Impac IP140. The pyrometer measures the emitted radiation intensity in the spectral range from 2 to 2.8 $\mu$m, and temperatures ranging from 100 to 700°C can be obtained. The pyrometer is equipped with focusing optics with a spot size of about 1.3 mm at a working distance of 150 mm. If the object is out of focus, the measurement spot size increases by about 0.1 mm per 1 mm working distance change in either direction. A smaller spot size would be possible if the working distance is decreased and the optics are replaced. However, in our experiments with a firing thruster, a smaller working distance is not feasible. The pyrometer is placed inside a vacuum-sealed housing, because the pyrometer is not specified for in-vacuum use. The housing is equipped with an infrared (IR) window made of Infrasil 301, which provides a high transmission over the whole measurement spectral range. The IR window is shielded by a shutter made of graphite, while the pyrometer is not operating. Typically, pyrometer line scans are performed with a scan velocity of 30 mm/s, and the pyrometer measures one data point every 0.3 mm. The pyrometer is calibrated using the measured emissivity of the graphite grid material and the transmission curve of the IR window. The pyrometer is tested in vacuum with a thermocalibrator made of graphite and equipped with a thermocouple. The measurement uncertainty is found to be 5°C.

A telemicroscope is used for high-resolution optical imaging of selected accelerator grid holes. The telemicroscope consists of a standard photographic lens with a focal length of 135 mm, an extension tube with a length of about 150 mm, and a charge-coupled device sensor with a resolution of $1360 \times 1024$ pixels [5]. The working distance of the telemicroscope is about 220 mm, the field of view is $5.8 \times 4.3$ mm$^2$, and the lateral resolution is found to be better than 0.01 mm. The telemicroscope is placed inside a separate vacuum-sealed housing with an optical viewport and a graphite shutter.

Surface profile scans are performed using a TLH Keyence L-KG 152 [5]. Using triangulation, the TLH precisely measures the distance between the measurement head and the measured object through a quartz viewport. The TLH can measure distances ranging from 110 to 190 mm. The reproducibility of the distance measurement is specified by the manufacturer to be better than 0.001 mm; due to the vibrations caused by the pumping system, the reproducibility is about 0.05 mm in our experiments. The TLH and the pyrometer are placed inside the same vacuum-sealed housing. The TLH uses a separate viewport with a quartz window and a separate shutter. The pyrometer and TLH are aligned such that their measurement spots are on a horizontal line with a horizontal distance of 67.5 mm. Upon that, horizontal temperature and surface profile scans can be performed simultaneously at the same vertical position. Because of the fixed position of the TLH and pyrometer relative to each other, the TLH distance measurements are used to monitor the position of the measured object relative to the focal plane of the pyrometer optics. Thus, the size of the measurement spot of the pyrometer on the object can be calculated.

The grid temperature cannot be measured directly, because the pyrometer spot covers the grid as well as the grid holes. Consequently, the pyrometer detects radiation emitted from the grid and from the background, such as radiation emitted by the discharge chamber and the plasma, when measuring the grid hole area. The portions of the detected radiation from the grid or from the background change with pyrometer position $y$. Hence, the pyrometer curve $T(y)$ is modulated with interferencelike structures.

To extract the accelerator grid surface temperature from the measured pyrometer data, we first calculate the area fraction $F$ of the measurement spot covering the grid surface versus horizontal position $y$. $F(y)$ depends on grid parameters (hole diameter $d_{\mathrm{Grid}}$ and hole distance $a_{\mathrm{Grid}}$) and scan parameters (spot diameter, vertical offset relative to grid center, and angle between scan line and a line of grid holes). Hole diameter and hole distance are obtained from the telemicroscopy images. The spot diameter is calculated from the TLH distance measurements. The two unknown scan parameters (vertical offset relative to grid center and angle between scan line and the line of grid holes) are varied until the area fraction curve $F(y)$ reproduces the interferencelike structures of the measured temperature curve $T(y)$ best.

The pyrometer detects the integrated intensity of the emitted radiation in the spectral range from 2.0 to 2.8 $\mu$m, which is given by

$$I(T) = \int_{2.0\ \mu\mathrm{m}}^{2.8\ \mu\mathrm{m}} t(\lambda) I'(\varepsilon, \lambda, T)\, \partial\lambda \tag{1}$$

where $t(\lambda)$ is the transmission of the IR window and $I'(\varepsilon, \lambda, T)$ is the radiation intensity emitted by the graphite surface of the accelerator grid. $I'(\varepsilon, \lambda, T)$ depends on the emissivity $\varepsilon$, the wavelength $\lambda$, and the temperature $T$. From Planck's law follows

$$I(T) = \int_{\lambda=2.0\ \mu\mathrm{m}}^{\lambda=2.8\ \mu\mathrm{m}} t(\lambda)\varepsilon(\lambda) \frac{c_1}{\pi n^2 \lambda^5} \left[\exp\left(\frac{c_2}{n\lambda T}\right) - 1\right]^{-1} \partial\lambda \tag{2}$$

where $n = 1$ is the refractive index of the ambient, and $c_1 = 3.7418\mathrm{E}-10$ Wm$^2$ and $c_2 = 1.4388\mathrm{E}-2$ mK are constants. The spectral emissivity of the grid material is measured, and the transmission of the IR window is given by the manufacturer. Both curves are plotted in Fig. 2. The relation between the displayed

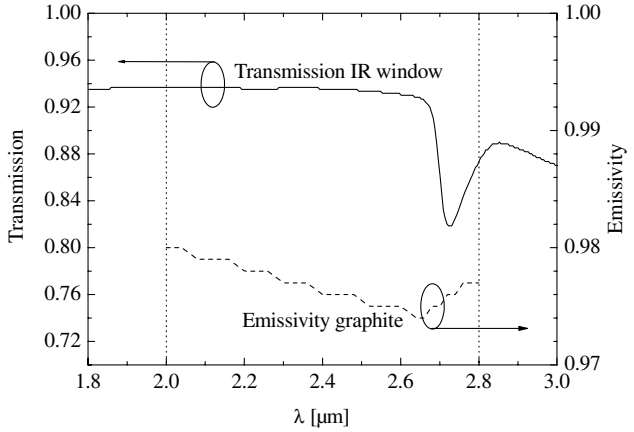


**Fig. 2 Spectral emissivity of graphite grid material (dashed line) and transmission curve of the IR window (solid line). Vertical dotted lines indicate spectral range in which the pyrometer detects emitted radiation intensity.**

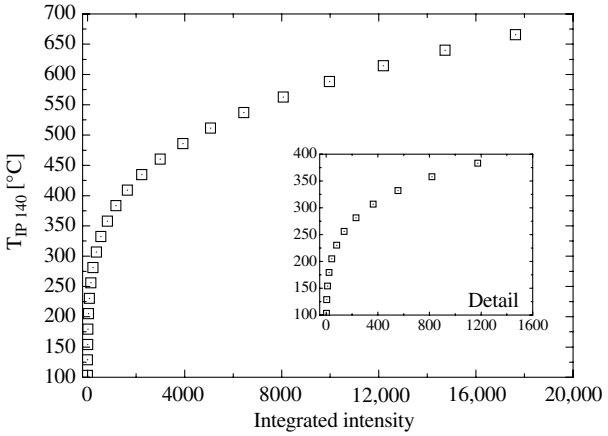


**Fig. 3 Calculated relation between displayed temperature $T_{IP140}$ and measured integrated intensity $I'(\varepsilon, \lambda, T)$ of pyrometer Impac IP 140 using the emissivity curve and transmission curve in Fig. 2.**

temperature and the obtained integrated intensity is depicted in Fig. 3. Here, a nonlinear behavior is found.

For the analysis of the experimental pyrometer data, the temperature curves $T(y)$ are converted into integrated intensity curves $I(y)$ using Eqs. (1) and (2). Then, the local maxima ($j = \max$) and local minima ($j = \min$) of the area fraction curve $[F_j(y)]$ and of the integrated intensity curve $[I_j(y)]$ are determined with respect to position $y$. Assuming that the detected radiation intensity is the sum of the radiation intensity emitted by the grid surface $I_{grid}$ and by the background $I_{back}$ weighted by their portions within the measurement spot of the pyrometer, it holds that

$$F_{max}(y)I_{grid}(y) + [1 - F_{max}(y)]I_{back}(y) = I_{max}(y) \quad (3)$$

$$F_{min}(y)I_{grid}(y) + [1 - F_{min}(y)]I_{back}(y) = I_{min}(y) \quad (4)$$

The linear system of equations can be solved, and the grid and background intensities can be calculated:

$$I_{grid}(y) = \frac{[1 - F_{min}(y)]I_{max}(y) - [1 - F_{max}(y)]I_{min}(y)}{[1 - F_{min}(y)]F_{max}(y) - [1 - F_{max}(y)]F_{min}(y)} \quad (5)$$

$$I_{back}(y) = \frac{F_{min}(y)I_{max}(y) - F_{max}(y)I_{min}(y)}{F_{min}(y)[1 - F_{max}(y)] - F_{max}(y)[1 - F_{min}(y)]} \quad (6)$$

Finally, the grid surface temperature can be calculated:

$$T_{grid}(y) = I^{-1}[I_{grid}(y)] \quad (7)$$

The calculation requires the use of the integrated intensity instead of the displayed temperature because of the nonlinear relation in Fig. 3. In principle, the temperature of the background could be calculated likewise, but it is difficult to define a background emissivity.

The test object is a radio-frequency-type ion thruster, RIT-22, developed by Astrium Space Transportation [15]. The discharge chamber diameter is 22 cm, and the beam diameter is 20 cm. The thruster is operated with Xe gas at three different beam power levels, as summarized in Table 1. The thruster is equipped with a two-grid system consisting of the inner screen grid and the outer accelerator grid. The holes of the accelerator grid are arranged in a hexagonal order, and their diameter is smaller than the diameter of the screen grid holes. The experiments are performed in a large vacuum test facility with a diameter of 3.8 m and a length of 11.5 m [15]. The pressure is about $6 \times 10^6$ mbar during thruster operation at a maximum total Xe flow of 34.25 standard $cm^3/min$.

The performed measurements are summarized in Table 2. Selected results are presented and discussed in the following section.

**Table 1 Main operation parameters of thruster**

| | Number | | |
|---|---|---|---|
| | I | II | III |
| Beam current, mA | 1000 | 1500 | 2000 |
| Beam power, W | 1250 | 2250 | 4000 |
| Beam voltage, V | 1250 | 1500 | 2000 |

## Results and Discussion

Figure 4 shows a telemicroscopy image of accelerator grid holes in the center of the thruster. The grid hole diameter is determined as 1.30 mm, the horizontal and vertical distances from grid hole center to grid hole center of the adjacent grid holes are $\Delta y_{hole} = 3.86$ mm and $\Delta z_{hole} = 2.225$ mm, respectively. In Fig. 5a, a TLH line scan across the diameter of the thruster is plotted. Because of the surface profile, the measurement spot size of the pyrometer changes with position, as shown in Fig. 5b. The TLH scan curve can also be employed to calculate the grid curvature, which is found to be $466.2 \pm 0.5$ mm for the cold thruster.

Measured pyrometer line scan curves of the thruster firing at 1250, 2250, and 4000 W beam power level are denoted in Fig. 6. The curves are modulated with interferencelike structures. The short period with $\Delta y_1 \sim 3.9$ mm is related to the horizontal distance between adjacent grid holes (see Fig. 4). The wider period with $\Delta y_2 \sim 33$ mm, which is responsible for the reduction of the oscillation amplitude at $y \sim 142$, 175, 208, 241, and 274 mm, is related to the fact that the scan line is not aligned parallel to a line of grid holes; that is, the scan line crosses several parallel lines of grid holes. The experiments show that the scan line is tilted by approximately 1.9° $[\arctan(0.5 \times \Delta z_{hole}/\Delta y_2)]$ with respect to a line of grid holes. The obtained pyrometer line scan curves are not symmetrical with respect to the horizontal grid center, because the scan line does not cross the grid center. The vertical offset increases from 2.84 to 3.02 mm with increasing operation time and increasing beam power level. The change of the vertical offset is related to the thermal expansion of the thruster.

The best-fit calculated area fraction curves, which correspond to the measured pyrometer curves in Fig. 6, are plotted in Fig. 7. Figure 8 shows the calculated grid surface temperature data at the three beam power levels. As expected, the calculated grid surface temperature increases toward the grid center. The calculated grid surface temperatures at the left and right ends correlate well with the temperatures obtained at the rim of the grid, i.e., next to the grid hole area where the pyrometer spot covers the grid completely. This agreement supports the correctness of our calculations. The temperature in the center of the grid is about 40°C higher than the temperature at the extremities. The uncertainty of the calculated

**Table 2 List of performed in situ measurements**

| Thruster state | Pyrometer | Telemicroscope | TLH |
|---|---|---|---|
| Thruster off | —— | X | X |
| Thruster firing at 1250 W | X | —— | X |
| Thruster firing at 2250 W | X | —— | X |
| Thruster firing at 4000 W | X | —— | X |
| Thruster warm up while firing at 1250 W | X | —— | X |
| Thruster cool-down phase after firing at 1250 W | X | —— | X |

**Table 3 Obtained accelerator grid surface temperatures**

| Beam power, W | Grid center, T, °C | Left rim of grid, T, °C |
|---|---|---|
| 1250 | $227 \pm 8$ | $187 \pm 5$ |
| 2250 | $263 \pm 8$ | $225 \pm 5$ |
| 4000 | $301 \pm 8$ | $255 \pm 5$ |

[a]Grid center temperatures are taken from results of the model calculation, and rim temperatures are taken from pyrometer line scans.

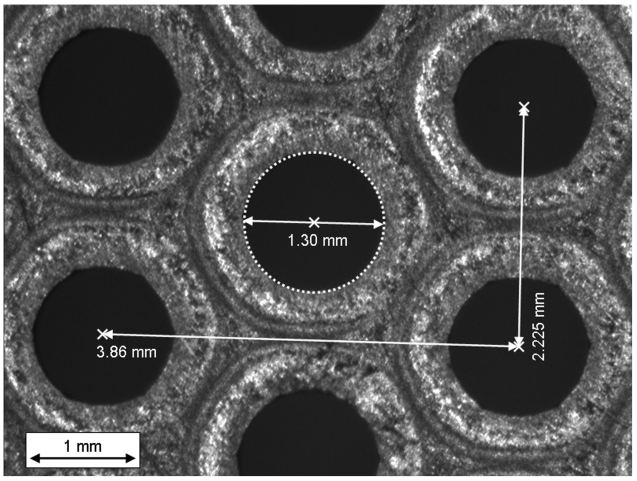


**Fig. 4 Telemicroscopy image of accelerator grid (grid center).**

temperatures is estimated from the analysis of multiple measurements performed at the same thruster operation parameters. It is found to be about 8°C.

Table 3 summarizes the calculated and measured grid surface temperatures for the grid center and left rim of the grid, respectively. In Fig. 9, the calculated and measured grid surface temperatures versus beam current are plotted. An almost linear relation can be seen for our data. Figure 9 also contains grid temperature data from [8,11,14]. Oglebay [8] published analytical temperature data of the

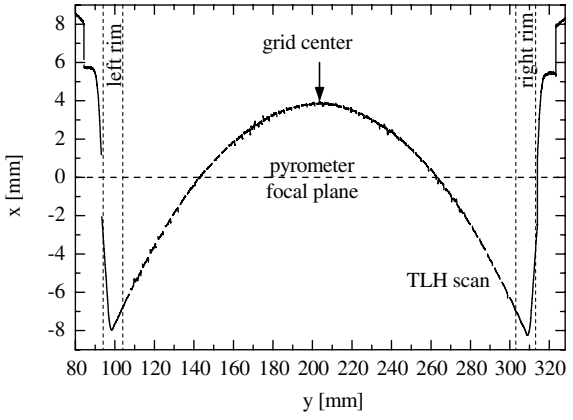


a)

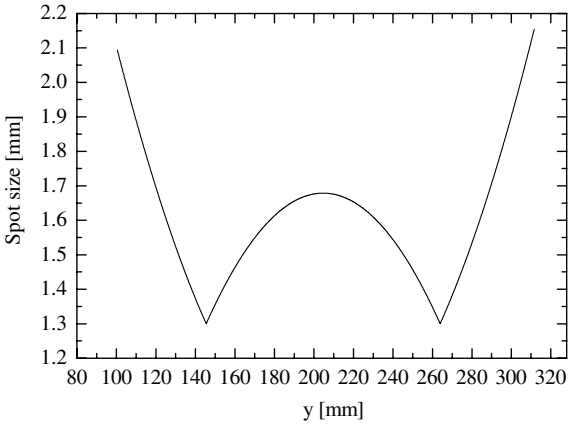


b)

**Fig. 5 TLH scan results: a) surface profile of accelerator grid (data are given relative to focal plane of pyrometer indicated by the dashed horizontal line at $x = 0$ mm); and b) calculated pyrometer spot size diameter.**

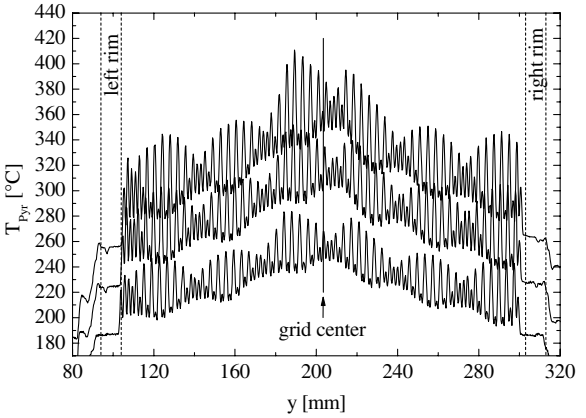


**Fig. 6 Measured pyrometer scan curves of RIT-22 operated at 1250 W (bottom), 2250 W (center), and 4000 W (top) beam power.**

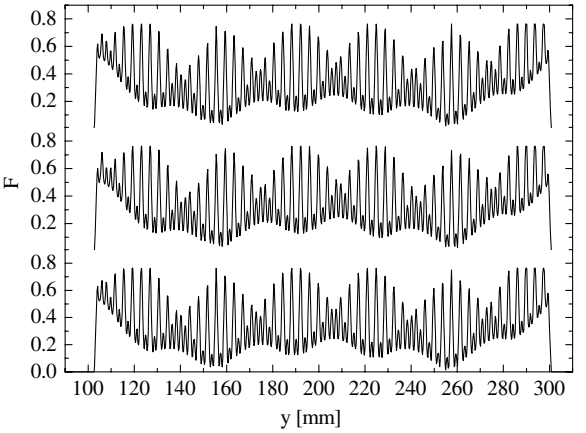


**Fig. 7 Best-fit simulated area fraction curves corresponding to pyrometer scan curves in Fig. 6 (bottom: 1250 W; center: 2250 W; and top: 4000 W).**

accelerator and screen grid assembly of a 30 cm Kaufman-type mercury ion thruster. These data agree well with our grid center data. Reference [11] contains experimental data of the accelerator grid ring of the NSTAR Kaufman-type ion thruster; [14] presents experimental data of the accelerator grid support of the NEXT Kaufman-type ion thruster. These data are considerably lower than the data reported here for the rim of the grid. We suppose that this difference can be attributed to different measurement positions in [11,14]

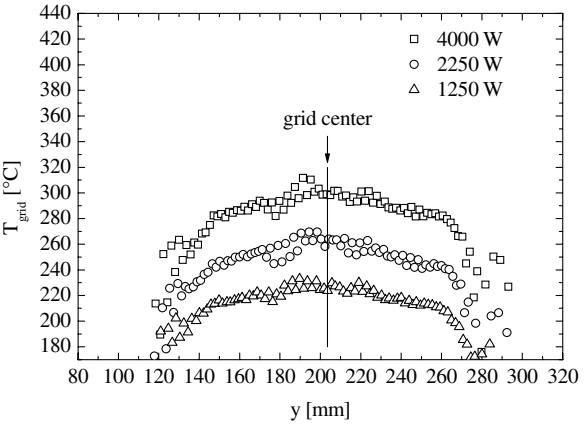


**Fig. 8 Grid surface temperature of RIT-22 at different beam power levels (bottom: 1250 W; center: 2250 W; and top: 4000 W). Data are calculated using pyrometer curves in Fig. 6 and area fraction curves in Fig. 7.**

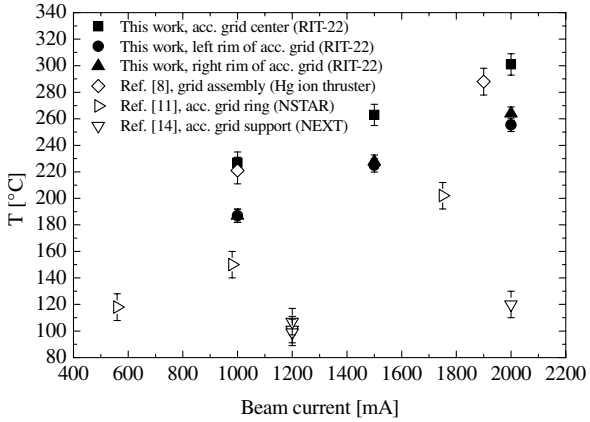


**Fig. 9 Calculated and measured temperatures (acc. denotes accelerator). Open symbols show analytical [8] and experimental [11,14] grid temperature data published by other groups for different measurement positions on grids of different Kaufman-type ion thrusters.**

compared with our study. The measurement spots in [11,14] seem to be further away from the grid hole area. However, the data in [8,11] suggest a similar increase of the reported temperature data with increasing beam current.

It can also be seen in Fig. 9 that the temperature at the right rim of the grid is slightly higher than at the left rim of the grid, especially at the highest beam power level. This difference is due to interactions of the thruster with the diagnostics; that is, the IR window in front of the pyrometer optics is heated up by the ion beam. Consequently, the IR window emits additional IR radiation that subsumes the radiation emitted by the thruster. For the smaller beam power levels, the difference is well below the measurement uncertainty of about 5°C.

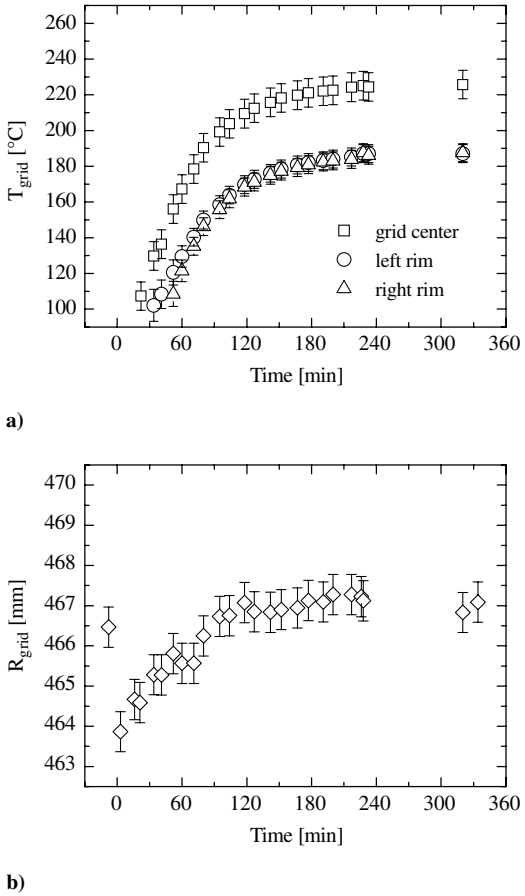


**Fig. 10 RIT-22 while warming up at a beam power level of 1250 W: a) grid surface temperatures and b) grid curvature. At $t = 0$ min, beam extraction is switched on.**

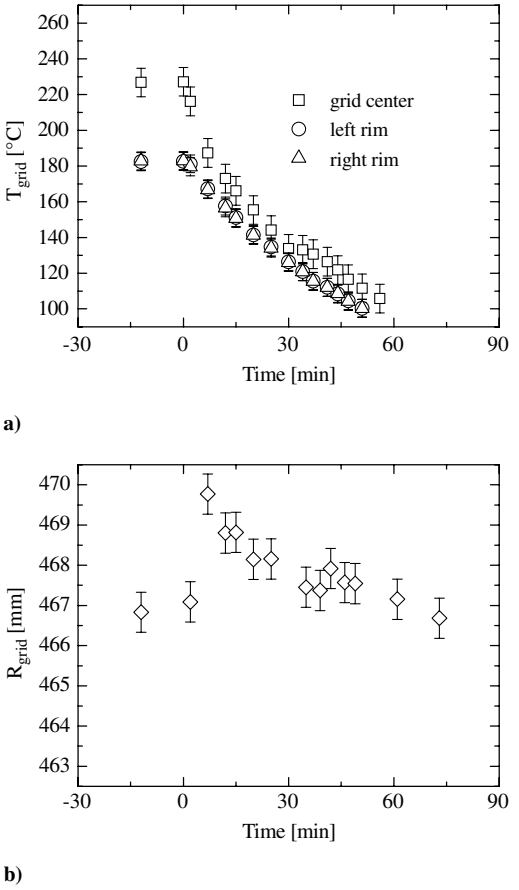


**Fig. 11 RIT-22 while cooling down after operation at a beam power level of 1250 W: a) grid surface temperatures and b) grid curvature. At $t = 0$ min, the beam and plasma are switched off.**

In situ temperature data of the thruster during warm-up and cool-down phases are demonstrated in Figs. 10a and 11a, respectively. The thruster is firing at a beam power level of 1250 W during the warm-up phase. The accelerator grid surface temperature changes systematically with time during the warm-up phase and cool-down phase, and the accelerator grid reaches thermal steady state after about 4 h of firing.

Simultaneously, TLH scans are performed and the grid curvature is monitored. The curvature data are plotted in Figs. 10b and 11b for the warm-up and cool-down phases, respectively. The grid curvature decreases or increases abruptly upon switching the beam voltage on or off, respectively, and subsequently relaxes. The abrupt change can be attributed to electrostatic forces between the screen and accelerator grid, which slightly increase the grid spacing [16]. With increasing firing time, the whole thruster expands due to rising temperature, which leads to relaxation of the grid curvature. Unfortunately, the grid gap cannot be determined from our experimental data. To measure the grid gap, modifications of the grids and the experimental setup are needed [16]. However, the grid curvature change is very small. Thus, we believe that the effect on the ion optics is negligible. Future activities should investigate this behavior.

## Conclusions

In summary, it has been demonstrated that the in situ diagnostic system can be employed for the in situ thermal characterization of EP thrusters. The determination of the surface temperature of the accelerator grid of a gridded ion thruster is exemplarily described, which is a very challenging task. In situ pyrometer line scans in combination with precise in situ measurements of geometrical grid parameters were performed. The accelerator grid surface temperature distribution was obtained from the pyrometer line scan curves by a model calculation that used appropriate equations and the measured

geometrical grid parameters. The measured temperature data are essential parameters for evaluating the performance of the thruster and for validated thruster modeling, which is an interesting task for future activities. It is supposed that the diagnostic system is an interesting tool for thermal characterization of other EP thruster types and parts. Recently, the characterization of a Hall-effect thruster SPT-100D EM1 was described, where (among others) the temperature of the plasma channel wall was measured [5]. In principle, the diagnostic system can be used to study the surface temperature of any optically accessible thruster part.

## Acknowledgments

The authors acknowledge financial support from ESA/European Space Research and Technology Centre within the project "Development of Advanced EP Thruster Characterization Diagnostics" (contract no. 20461/06/NL/CP). The authors are deeply grateful to their project coordinators, P.-E. Frigot and J. Gonzalez del Amo.

## References

[1] Goebel, D. M., and Katz, I., *Fundamentals of Electric Propulsion: Ion and Hall Thrusters*, JPL Space Science and Technology Series, Vol. 1, Wiley, New York, 2008, p. 1.

[2] Choueiri, E. Y., "A Critical History of Electric Propulsion: The First 50 Years (1906–1956)," *Journal of Propulsion and Power*, Vol. 20, No. 2, 2004, pp. 193–203. doi:10.2514/1.9245

[3] Jahn, R. G., and Choueiri, E. Y., *Encyclopedia of Physical Science and Technology*, Vol. 5, Academic Press, San Diego, CA, 2001, pp. 125–141.

[4] Marcucci, M. G., and Polk, J. E., "NSTAR Xenon Ion Thruster on Deep Space 1: Ground and Flight Tests (invited)," *Review of Scientific Instruments* Vol. 71, No. 3, 2000, pp. 1389–1400. doi:10.1063/1.1150468

[5] Bundesmann, C., Tartz, M., Scholze, F., Leiter, H. J., Scortecci, F., Gnizdor, R. Y., and Neumann, H., "Note: An Advanced In Situ Diagnostic System for Characterization of Electric Propulsion Thrusters and Ion Beam Sources," *Review of Scientific Instruments*, Vol. 81, No. 4, 2010, Paper 046106. doi:10.1063/1.3386585

[6] Wen, L., Crotty, J. D., and Pawlik, E. V., "Ion Thruster Thermal Characteristics and Performance," *Journal of Spacecraft and Rockets*, Vol. 10, No. 1, 1973, pp. 35–41. doi:10.2514/3.61844

[7] Mirtich, M. J., "The Effects of Exposure to LN2 Temperatures and 2.5 Suns Solar Radiation on 30-cm Ion Thruster Performance," NASA TM X-71652, 1975.

[8] Oglebay, J. C., "Thermal Analytical Model of a 30cm EM Mercury Ion Thruster," NASA TM X-71680, 1975.

[9] Rawlin, V. K., Patterson, M. J., and Becker, R. A., "Thermal Environmental Testing of NSTAR Engineering Model Ion Thrusters," 25th International Electric Propulsion Conference, Cleveland, OH, IEPC Paper 1997-051, Electric Rocket Propulsion Soc., Fairview Park, OH, Aug. 1997.

[10] Van Noord, J., Gallimore, A., and Rawlin, V. K., "Numerical Thermal Model of a 30-cm NSTAR Ion Thruster," 25th International Electric Propulsion Conference, Cleveland, OH, IEPC Paper 1997-185, Electric Rocket Propulsion Soc., Fairview Park, OH, Aug. 1997.

[11] Van Noord, J. L., Gallimore, A., and Rawlin, V. K., "Numerical Thermal Model of NASA Solar Electric Propulsion Technology Application Readiness Ion Thruster," *Journal of Propulsion and Power*, Vol. 16, No. 2, 2000, pp. 357–364. doi:10.2514/2.5577

[12] Sarver-Verhey, T. R., Domonkos, M. T., and Patterson, M. J., "Thermal Characterization of a NASA 30-cm Ion Thruster Operated up to 5 kW," 36th AIAA Joint Propulsion Conference, Huntsville, AL, AIAA Paper 2000-3816, July 2000.

[13] Anderson, J. R., Snyder, J. S., Van Noord J. L., and Soulas, G. C., "Thermal Development Test of the NEXT PM1 Ion Engine," 43rd AIAA Joint Propulsion Conference, Cincinnati, OH, AIAA Paper 2007-5217, July 2007.

[14] Van Noord, J. L., "NEXT Ion Thruster Thermal Model," 43rd AIAA Joint Propulsion Conference, Cincinnati, OH, AIAA Paper 2007-5218, July 2007.

[15] Leiter, H. J., Kukies, R., Killinger, R., Bonelli, E., Scaranzin, S., Scortecci, F., Neumann, H., and Tartz, M., "RIT-22 Ion Propulsion System: 5000 h Endurance Test Results and Life Prediction," 43rd AIAA Joint Propulsion Conference, Cincinnati, OH, AIAA Paper 2007-5198, July 2007.

[16] Soulas, G. C., and Frandina, M. M., "Ion Engine Grid Gap Measurements," 40th AIAA Joint Propulsion Conference, Fort Lauderdale, FL, AIAA Paper 2004-3961, July 2004.

L. King
*Associate Editor*